Krauskopf, B., & Oldeman, B. E. (2006). Bifurcations of global reinjection orbits near a saddle-node Hopf bifurcation.

Bifurcations of global reinjection orbits near a saddle-node Hopf bifurcation

Bernd Krauskopf

Department of Engineering Mathematics, University of Bristol, University Walk, Bristol BS8 1TR, United Kingdom

E-mail: B.Krauskopf@bristol.ac.uk

Bart E. Oldeman

Department of Mathematics, University of Auckland, Private Bag 92019, Auckland, New Zealand

E-mail: oldeman@math.auckland.ac.uk

May 2006

Abstract. The saddle-node Hopf bifurcation (SNH) is a generic codimension-two bifurcation of equilibria of vector fields in dimension at least three. It has been identified as an organizing centre in numerous vector field models arising in applications. We consider here the case that there is a global reinjection mechanism, because the centre manifold of the zero eigenvalue returns to a neighbourhood of the equilibrium. Such a SNH bifurcation with global reinjection occurs naturally in applications, most notably in models of semiconductor lasers.

We construct a three-dimensional model vector field that allows us to study the possible dynamics near a SNH bifurcation with global reinjection. This model follows on from our earlier results on a planar (averaged) vector field model, and it allows us to find periodic and homoclinic orbits with global excursions out of and back into a neighbourhood of the SNH point. Specifically, we use numerical continuation techniques to find a two-parameter bifurcation diagram for a well known and complicated case of a SNH bifurcation that involves the break-up of an invariant sphere. As a particular feature we find a concrete example of a phenomena that was studied theoretically by Rademacher: a curve of homoclinic orbits that accumulates on a segment in parameter space while the homoclinic orbit itself approaches a saddle periodic orbit.

AMS classification scheme numbers: 37G10 37G15 34C14 34C37 34C60

1. Introduction

A saddle-node Hopf (SNH) bifurcation is one of the basic codimension-two bifurcations of equilibria of vector fields. As the name indicates, it is a simultaneous saddle-node and Hopf bifurcation, characterized by the fact that the linearization about the equilibrium has one real zero and a pair of purely imaginary complex conjugate eigenvalues. The SNH bifurcation has a three-dimensional center manifold — it is generically expected in any vector field of dimension at least three when two parameters can be varied independently. Indeed the SNH bifurcation is one of the 'classic' codimension-two bifurcations. It has been found as an organising center in numerous applications (for example, in [3, 16, 20, 21, 26, 27, 24, 28, 30, 32]) and is discussed in standard textbooks on bifurcation theory, such as [9, 12, 19]. It is well known that complicated dynamics, for example, curves of Shil'nikov homoclinic orbits to saddle foci [4, 6, 11, 13], can be found in a local neighbourhood of a SNH point.

We are interested here in the situation that the SNH point comes with a global reinjection mechanism. This is motivated by the discovery of periodic and homoclinic orbits that feature global excursions out of and back into a neighbourhood of a SNH point. Our direct motivating example is a semiconductor laser with optical injection, which has a global reinjection mechanism that corresponds to a phase slip of the laser with respect to the injected light [30]. Periodic orbits that combine phase jumps with dynamics near a SNH point have been discussed in [18, 26, 30, 32]. However, such global reinjection orbits near a SNH bifurcation have also been found in dynamo theory [3] and, more abstractly, in a vector field approximation of a three-dimensional diffeomorphism with a region of weak resonance [28, Chapter 4.3.2].

In [15] we constructed and studied the $\mathbb{Z}_2$-symmetric *planar model vector field* for a SNH point with global reinjection

$$\begin{aligned} \dot{x} &= \nu_1 x - a x \sin\varphi - x^3 \\ \dot{\varphi} &= \nu_2 + s x^2 + 2\cos\varphi + c x^4 \,. \end{aligned} \tag{1}$$

Here x corresponds to the radial component associated with the Hopf bifurcation and reinjection is represented by the 2π-translationally symmetric variable φ. Owing to the symmetries, the planar model vector field is in fact a vector field on the half cylinder $\mathbb{R}^{\geq 0} \times \mathbb{S}^1$. Importantly, the circle $\mathbb{S}^1 = \{x = 0\}$ is invariant. In (1) a SNH point reduces to a saddle-node pitchfork (SNP) point. Reference [15] presents four different cases, A–D (depending on the higher-order coefficients a, s and c), of two-parameter unfoldings in the (ν_1, ν_2)-plane. In particular, we found periodic, homoclinic and families of heteroclinic orbits that wind around the half cylinder.

In this paper we consider bifurcations of periodic and homoclinic orbits near a SNH bifurcation with global reinjection *in the full three-dimensional setting*. Specifically, we concentrate on such orbits that involve one or more global excursions. The analysis of the SNP bifurcation in the planar model (1) is an important first step for understanding the dynamics. However, when one 'translates' the planar dynamics to the three-dimensional situation of a generic SNH bifurcation, one needs to add the azimuthal term and break

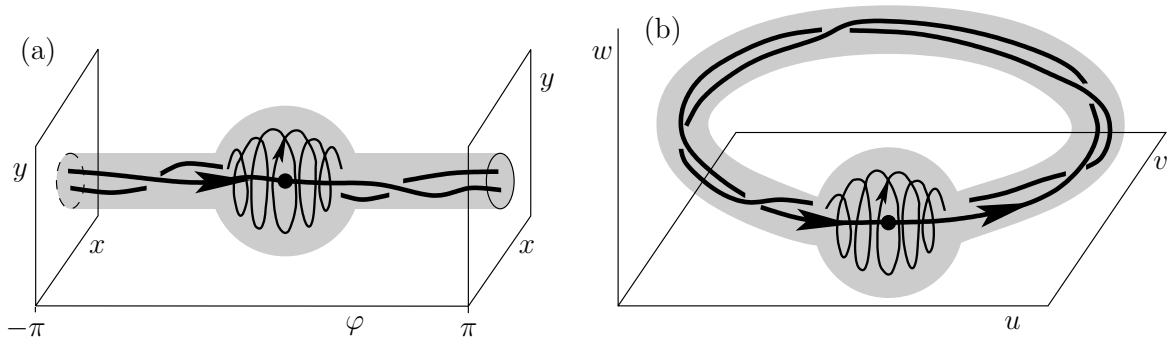

Figure 1. Neighbourhood of interest around a SNH point (of type III) with global reinjection of model vector field (2) in (x, y, φ)-space (a), and its embedding (6) in (u, v, w)-space (b).

the invariance of the invariant circle [12, 19]. As we will see, this breaking of the normal form symmetry has dramatic consequences for the full three-dimensional dynamics.

The key ingredient of our study is the construction (see section 2) of a *three-dimensional model vector field*, namely

$$\begin{aligned} \dot{z} &= (\nu_1 + \omega i)z - (\alpha + \beta i)z\sin\varphi - z|z|^2 + (d + fi)(2\cos\varphi + \nu_2)^2 \\ \dot{\varphi} &= \nu_2 + s|z|^2 + 2\cos\varphi + c|z|^4 \,. \end{aligned} \tag{2}$$

This system models a generic situation and allows us to study in detail the dynamics in a tubular neighbourhood of a SNH point with global reinjection; see figure 1. In particular, the two parameters d and f break the invariant circle $\mathbb{S}^1 = \{z = 0\}$ that exists for $d = f = 0$. For simplicity we set the azimuthal frequency to $\omega = 1$ and $\beta = 0$, so that α plays the same role as the coefficient a in (1).

There are two different classes of SNH points, depending on the way the centre manifold of the saddle-node Hopf bifurcation returns to the SNH point after the global excursion [15, figure 1]. The three types II(a), II(b) and IV(b) of SNH points (in the notation of [12]) occur on a generic invariant circle (even when the normal form symmetry is broken). For these types of SNH points the dynamics is effectively described already by the planar model (1). We concentrate here on the more interesting types I, III and IV(a), where the centre manifold of the saddle-node at the SNH point does not form an invariant circle. These three types of SNH points require a four-parameter unfolding in (ν_1, ν_2, d, f)-space, which is a highly nontrivial task.

We do not attempt a full unfolding here, but rather we perform a detailed study of the bifurcation diagram in the (ν_1, ν_2)-plane (for suitable $d \neq 0$ and $f \neq 0$) of the most interesting type III. The (local) SNH bifurcation of type III involves the break-up of an invariant sphere (in the normal form) [12, 19] and has been found as the organising centre in numerous applications; see, for example, [15, 17] for references. We consider here the dynamics in the full three-dimensional phase space that is associated with the unfolding of type A of the planar model (1) in [15], which contains a SNH point of type III. Specifically, we study the bifurcations of periodic and homoclinic orbits

with global excursions and reinjection. To this end we use numerical continuation with AUTO/HomCont [10] and homoclinic branch switching [22] to reveal an intriguing structure of homoclinic orbits with zero, one or more global excursions outside of and back into a neighborbood of the SNH point. As part of the unfolding of type A we also encounter a SNH bifurcation of type I, but we do not investigate it further because it does not involve any global reinjection orbits.

As a particular feature we find homoclinic orbits that accumulate on a saddle periodic orbit of the system. At the same time the curve in parameter space of the respective homoclinic bifurcation accumulates on a segment. This phenomenon was studied theoretically in [23], and we present here a concrete example of the associated bifurcation structure. We find good agreement with the theory, including the theoretical scaling law of the accumulation process. Our results show that the phenomena in [23] can be expected near SNH points with global reinjection.

This paper is organized as follows. In section 2 we provide background information on the construction of the model vector field (2), and in section 3 we present its local bifurcations. Section 4 is concerned with the global bifurcation structure. We start in section 4.1 with homoclinic orbits that do not leave a neighbourhood of the SNH point. Section 4.2 treats homoclinic orbits with one global reinjection and section 4.3 multi-reinjection homoclinic orbits. The accumulation phenomenon of homoclinic orbits is the topic of section 5. Finally, in section 6 we conclude and point out open problems.

2. Derivation of the model vector field

The planar model vector field (1) was constructed in [15] by starting from the unfolding of a (local) SNH point [12, 19] in cylindrical co-ordinates and leaving off the azimuthal term describing the rotation due to the Hopf bifurcation. This gives a $\mathbb{Z}_2$-symmetric planar vector field approximation, whose four-jet [17] has the form

$$\begin{aligned} \dot{x} &= \mu_1 x - axy - x^3 \\ \dot{y} &= \mu_2 + sx^2 - y^2 + bx^4 \,. \end{aligned} \tag{3}$$

Global reinjection is then introduced by replacing y in (3) with the 2π-periodic variable φ. A convenient choice of trigonometric terms gives the $\mathbb{Z}_2$-symmetric planar model (1). System (1) has two SNP points on the invariant circle $\mathbb{S}^1 = \{x = 0\}$, namely SNP^+ at $(x, \varphi) = (0, 0)$ and SNP^- at $(x, \varphi) = (0, \pi)$ for $(\nu_1, \nu_2) = (0, \pm 2)$. The bifurcation diagram in the (ν_1, ν_2)-plane of (1) connects SNP^+ and SNP^-. Locally near these codimension-two bifurcation points one retrieves the local bifurcation structure of a SNP point; which case one is dealing with depends on the higher order coefficients a, s, and c. Importantly, the points SNP^+ and SNP^- differ in the sign of s, so that the unfoldings of the planar model (1) are closely related to the unfolding in [17] of the codimension-three degenerate SNP bifurcation given by $s = 0$ in (3).

In order to construct the three-dimensional vector field model (2) we consider the normal form near a local SNH point that includes the azimuthal term. It is best written

in terms of a complex variable $z \in \mathbb{C}$ [19], and has the four-jet

$$\begin{aligned} \dot{z} &= (\nu_1 + \omega i)z - (\alpha + \beta i)zy - z|z|^2 \\ \dot{y} &= \nu_2 + s|z|^2 - y^2 + b|z|^4. \end{aligned} \tag{4}$$

Global reinjection is then again introduced by replacing y in (3) with the 2π-periodic variable φ. The same convenient choice of trigonometric terms as in [15] gives the vector field

$$\begin{aligned} \dot{z} &= (\nu_1 + \omega i)z - (\alpha + \beta i)z\sin\varphi - z|z|^2 \\ \dot{\varphi} &= \nu_2 + s|z|^2 + 2\cos\varphi + c|z|^4. \end{aligned} \tag{5}$$

We remark that (5) can be obtained from (1) formally by replacing x by z, x^2 by $|z|^2$, ν_1 by $\nu_1 + \omega i$, and a by $\alpha + \beta i$. System (5) is a vector field on the cylinder $\mathbb{C} \times \mathbb{S}^1$. Importantly, due to the normal form construction the circle $\mathbb{S}^1 = \{z = 0\}$ is invariant. This means that (5) only describes the dynamics near a SNH point with global reinjection in the non-generic case that there is an extra symmetry that forces this invariance; for an example of such a system see [3].

The final step in our construction is, hence, the addition of terms that break the invariance of $\mathbb{S}^1$ in (5). This can be done in many ways, but a particularly convenient choice is to add the term $(d+fi)(2\cos\varphi+\nu_2)^2$ to the equation for $\dot{z}$, which gives (2). The factor $(2\cos\varphi + \nu_2)^2$ vanishes exactly when $\dot{\varphi}|_{z=0} = 0$, which ensures that the equilibria of the model (2) occur for $z = 0$. In other words, while the invariant circle is broken, these equilibria are at the same positions as in (5). This greatly simplifies the analysis, as well as setting up of numerical computations of homoclinic orbits.

By setting $z = x + iy$, system (2) can be written as

$$\begin{aligned} \dot{x} &= \nu_1 x - \omega y - (\alpha x - \beta y)\sin\varphi - (x^2 + y^2)x + d(2\cos\varphi + \nu_2)^2 \\ \dot{y} &= \nu_1 y + \omega x - (\alpha y + \beta x)\sin\varphi - (x^2 + y^2)y + f(2\cos\varphi + \nu_2)^2 \\ \dot{\varphi} &= \nu_2 + s(x^2 + y^2) + 2\cos\varphi + c(x^2 + y^2)^2 \end{aligned} \tag{6}$$

which is the form we use in the analysis and for numerical calculations.

It is convenient to represent global periodic and homoclinic orbits of (2) in $\mathbb{R}^3$, so that it is immediately clear how they close up. This can be achieved by mapping the φ-axis onto a circle with sufficiently large radius R. We use the transformation

$$\begin{aligned} u &= (R + x)\cos\varphi \\ v &= (R + x)\sin\varphi \\ w &= y \end{aligned} \tag{7}$$

where we use $R = 2$, which ensures that the image of a sufficiently large tubular neighbourhood of the reinjection loop does not self-intersect; see figure 1.

3. Local bifurcation analysis

Due to the choice of the term that breaks the invariance of the circle $\mathbb{S}^1 = \{z = 0\}$, system (2) has the same structure of local bifurcations as the planar system (1).

Lemma 1. *For any values of d and f the vector field model (2) has the following local bifurcations:*

(i) two lines, given by $\nu_2 = \pm 2$, of saddle-node bifurcations S_0. At S_0 two equilibria, denoted a and b, with $z = 0$ are born that exist for $|\nu_2| < 2$;

(ii) an ellipse of Hopf bifurcations H given by

$$\left(\frac{\nu_1}{\alpha}\right)^2 + \left(\frac{\nu_2}{2}\right)^2 = 1;$$

(iii) the curves S_0 and H are tangent at two SNH points, namely SNH^+ at $(z, \varphi) = (0, 0)$ and SNH^- at $(z, \varphi) = (0, \pi)$. At SNH^+ the sign of the coefficient s of the planar four-jet normal form (3) is positive and at SNH^- it is negative.

Proof. There are two equilibria of (2) for $z = 0$ whose φ-values are given by $\nu_2 = -2\cos\varphi$. In other words, these equilibria exists for $|\nu_2| < 2$, and for $\nu_2 = \pm 2$ there is only a single equilibrium at $\varphi = 0$ and $\varphi = \pi$, respectively. At the equilibria the Jacobian of (6) is given by

$$\begin{pmatrix} \nu_1 - \alpha\sin\varphi & -\omega + \beta\sin\varphi & 0 \\ \omega - \beta\sin\varphi & \nu_1 - \alpha\sin\varphi & 0 \\ 0 & 0 & -2\sin\varphi \end{pmatrix}$$

with characteristic equation

$$((\nu_1 - \alpha - \lambda)^2 + (\omega - \beta\sin\varphi)^2)(-2\sin\varphi - \lambda) = 0\,.$$

The eigenvalues are given by

$$\begin{aligned} \lambda_1 &= -2\sin\varphi = \pm 2\sqrt{1 - \frac{{\nu_2}^2}{2}} \quad \text{and} \\ \lambda_{2,3} &= \pm i(\omega - \beta\sin\varphi) - \nu_1 + \alpha\sin\varphi\,. \end{aligned}$$

We conclude that for $\nu_2 = \pm 2$ indeed $\lambda_1 = 0$, which proves part (i).

Furthermore, $\lambda_{2,3}$ is a pair of purely imaginary eigenvalues if and only if

$$\sin\varphi = \frac{\nu_1}{\alpha}\,,$$

which, with $\nu_2 = -2\cos\varphi$, gives part (ii).

Combining (i) and (ii) gives the location of SNH^+ and SNH^-. The sign of s in the planar four-jet normal form (3) follows from [15, Lemma 2], because by construction the points SNH^+ and SNH^- reduce to the points SNP^+ and SNP^- of (1). This completes part (iii). □

4. Analysis of global bifurcations

For the planar model vector field (1) it is possible to determine analytically saddle-node bifurcation curves of equilibria off the invariant circle. In the three-dimensional model (2) this bifurcation corresponds to a saddle-node bifurcation of periodic orbits. Hence, the respective curves S_l of (2) cannot be found analytically, but only by numerical continuation. See already figure 2(a) for the arrangement of the curves S_0, H and S_l, which form the basic structure of the bifurcation diagram of (2).

Throughout we use the software AUTO/HomCont [10] to find and follow curves of global bifurcations. AUTO is a numerical bifurcation analysis package, which uses pseudo-arclength continuation in combination with the solution of two-point boundary value problems with Gauss-Legendre collocation. The periodic and homoclinic orbits under consideration in this paper are discretized with a total of `NTST`×`NCOL` points, where `NTST` is the number of basic mesh points and `NCOL` is the number of so-called Gauss collocation points per mesh interval. We keep `NCOL`=4 fixed and vary `NTST` between 100 and 700 depending on the complexity of the orbit.

From now on we restrict our attention to the unfolding of type A of [15], which contains a SNH point of type III (in the notation of [12]) as the point SNH^-, and a SNH point of type I as the point SNH^+. To this end we set $\alpha = -1$, $s = -1$ and $c = 0$ in (2); recall that $\omega = 1$ and $\beta = 0$. We found that it is important to have both $d \neq 0$ and $f \neq 0$ to break the invariance of the circle $\mathbb{S}^1 = \{z = 0\}$ and to avoid the case $d = f$ (and possibly other ratios). Since we are not attempting an unfolding in d and f we set $f = \pi d$ and consider the bifurcation diagram in the (ν_1, ν_2)-plane for different values of d. We remark that there is a trade-off in choosing d. If d is too small then all bifurcation curves and orbits are very close to each other and hard to compute and distinguish. However, if d is too large then one may encounter bifurcations that are not directly due to the SNH bifurcation with global reinjection. We found that the value of $d = 0.01$ is suitable from this point of view.

As was explained in the introduction, our main interest is in finding the bifurcation structure of global reinjection homoclinic orbits. Throughout this paper we distinguish by superscripts, a and b, between curves h of orbits that are homoclinic to either of the two different saddle foci. Furthermore, superscripts indicate the number of global excursions that occur along the homoclinic orbit.

4.1. Local part of the bifurcation diagram

Figure 2 shows the part of the bifurcation diagram that is as is expected from unfolding A of the planar vector field model (1) in [15]. First of all, there are the curves S_0 and H that meet at the points SNH^+ and SNH^- as described by Lemma 1. Shown are also the curves S_l of saddle-node of limit cycle bifurcations, which end at the curve H in degenerate Hopf bifurcation points. Emerging from the point SNH^- is a curve T of torus (Neimark-Sacker) bifurcations. It ends on S_l in a 1:1 resonance point (also called Bogdanov-Takens bifurcation of the return map) [2, 5]. It is known from the literature

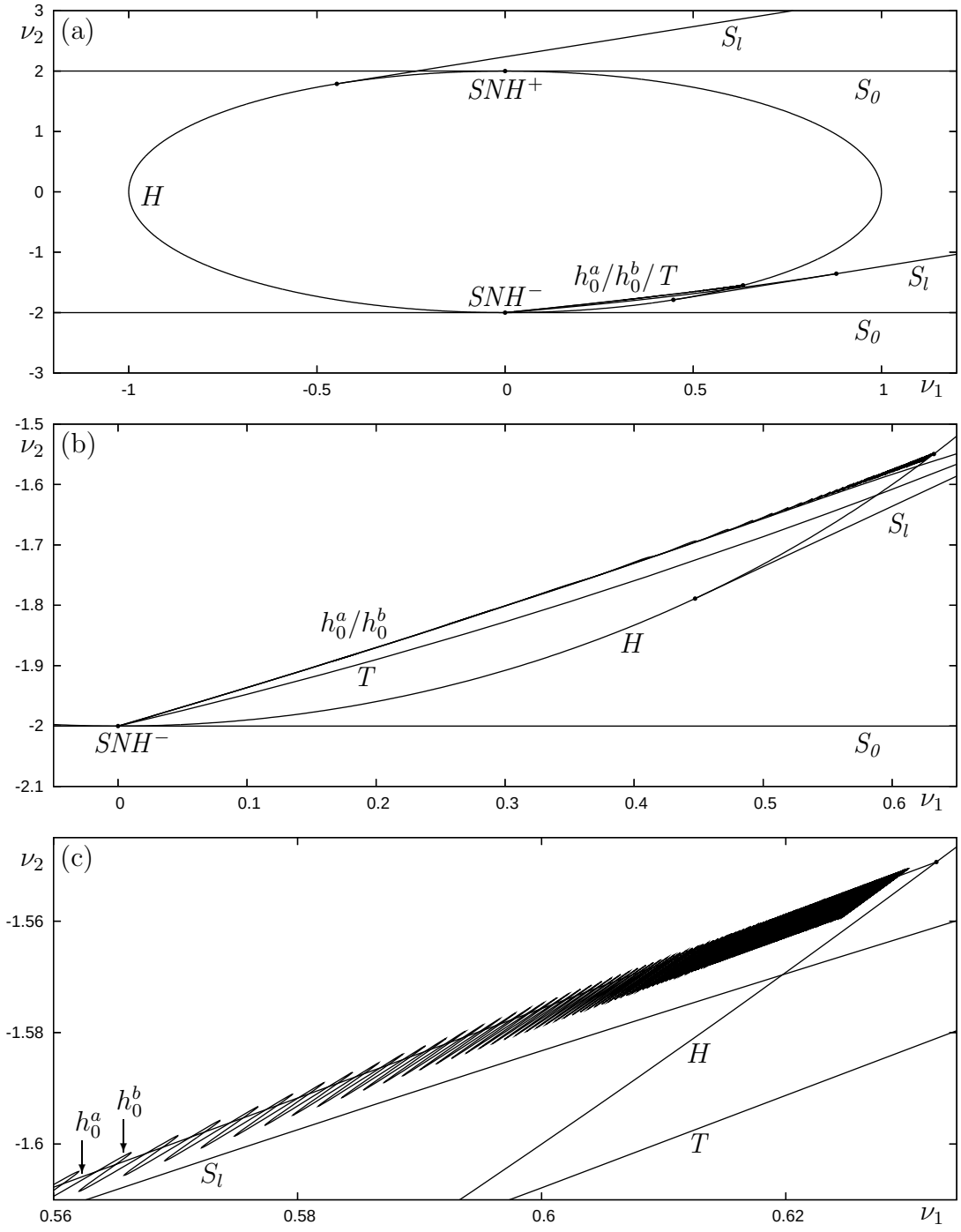

Figure 2. Bifurcation diagram in the (ν_1, ν_2)-plane for $d = 0.01$ (a) and two enlargements (b) and (c). Shown are saddle-node bifurcation curves S_0, Hopf bifurcation curve H, saddle-node bifurcation of limit cycle curves S_l, torus bifurcation curve T, and homoclinic bifurcation curves h_0^a and h_0^b.

(for case III of a SNH bifurcation [12, 19]) that there is a curve C of heteroclinic bifurcations between the two saddles in the planar normal form; see also [17]. In the full three-dimensional situation this single curve splits up into four curves: a pair h_0^a and h_0^b

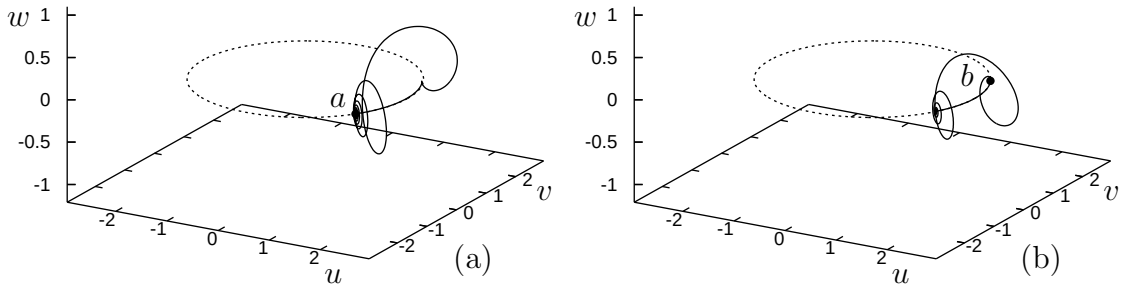

Figure 3. Homoclinic orbits of types h_0^a (a) and h_0^b (b) for $d = 0.01$ in (u, v, w)-space of (7); the dashed curve is the circle $\mathbb{S}^1 = \{z = 0\}$.

of homoclinic orbits of the saddle foci a and b, respectively, and a pair of heteroclinic orbits (which we do not investigate in this paper). These homoclinic orbits stay inside the neighbourhood of the SNH point, that is, do not involve a global excursion. Phase portraits of homoclinic orbits of type h_0^a and h_0^b are shown in figure 3. Notice that both homoclinic orbits of type h_0^a and h_0^b have a section that follows closely the circle $\mathbb{S}^1 = \{z = 0\}$ (dashed curve). This is because the parameter $d = 0.01$ that breaks the invariance of $\mathbb{S}^1$ is still quite small.

Note that general theory (see for instance [19, Ch 8.5]) predicts that the torus bifurcating from T only exists for nearby parameter values. The torus is destroyed if we move away from the curve. This occurs in a complex sequence of events that involves Arnol'd resonance tongues that emerge from point of rational rotation numbers on T. The Arnol'd tongues are beyond the scope of this paper and not shown in figure 2.

As is clear from the subsequent enlargement in figure 2(b) and (c), the curves h_0^a and h_0^b oscillate around each other, a phenomenon near a SNH point that has been studied in [6]. One-parameter continuation in ν_1 or ν_2 from a point on the curve h_0^a shows that the bifurcating periodic orbit undergoes several saddle-node bifurcations (S_l is one of them) and then disappears in a homoclinic bifurcation at curve h_0^b.

Figure 2(c) shows clearly that the curve h_0^b oscillates wildly around the curve h_0^a, which is almost a straight line away from SNH^-. The curve h_0^a ends at a homoclinic Hopf bifurcation point on the curve H, where the equilibrium a ceases to be a saddle focus. The equilibrium b does not undergo a Hopf bifurcation along H, but as the curve h_0^b gets closer to the Hopf bifurcation curve H the homoclinic orbit makes more and more loops near the point a; a few such loops are already visible in Fig. 3(b). As this happens the curve appears to accumulate on a line segment. During this accumulation process it becomes incresingly difficult to continue h_0^b numerically, and we were not able to continue the curve h_0^b further than shown. However, it seems plausible that this orbit, similar to the one that is discussed in more detail in section 5, accumulates on the saddle periodic orbit that bifurcates to the right hand side of curve H from equilibrium a.

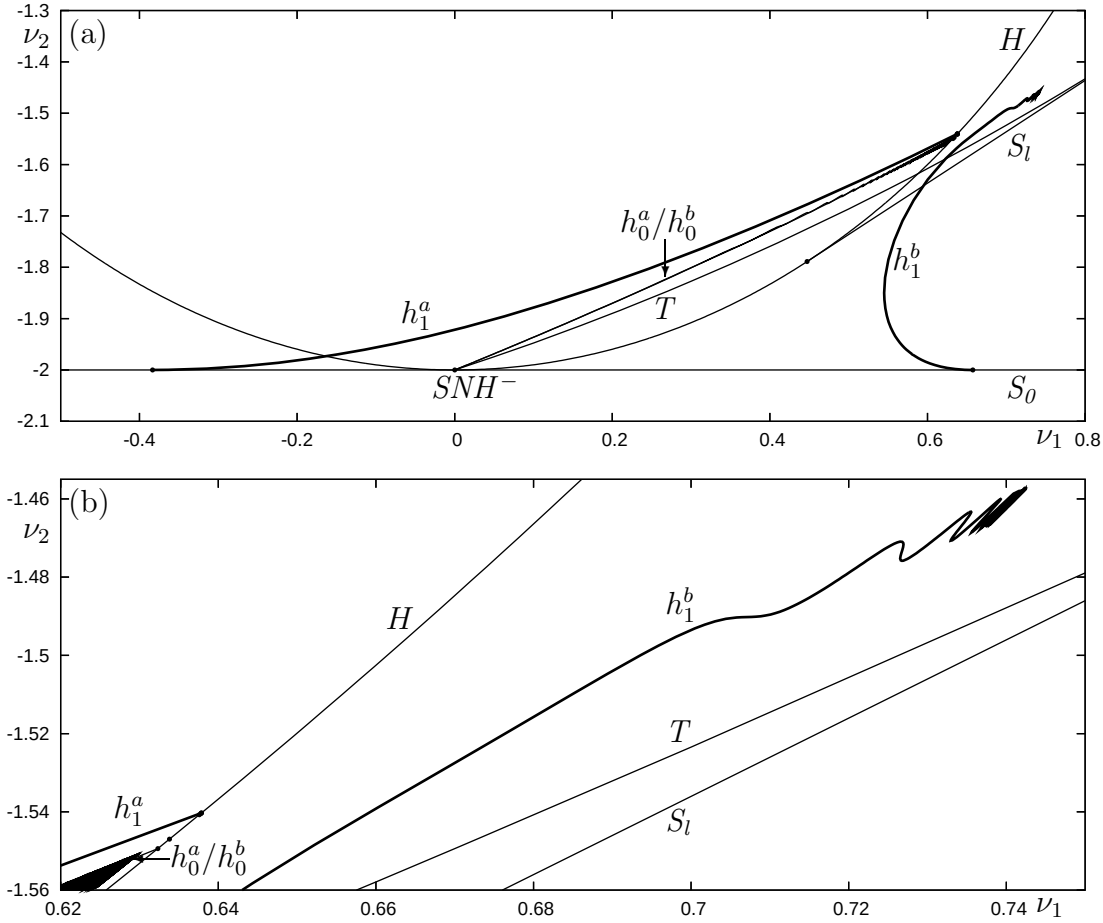

Figure 4. Bifurcation diagram in the (ν_1, ν_2)-plane near SNH^- for d=0.01 with curves h_1^a and h_1^b of homoclinic orbits with one global excursion. Panel (b) shows how the curves h_1^a and h_1^b terminate.

4.2. Homoclinic orbits with one global excursion

Figure 4 shows the bifurcation diagram for $d = 0.01$ near SNH^-, but now with two extra curves h_1^a and h_1^b of homoclinic orbits that make one global excursion. Figure 5(a) and (b) are phase portraits of homoclinic orbits of type h_1^a and h_1^b for this value of $d = 0.01$. Notice how the global excursion follows the (dashed) circle $\mathbb{S}^1$. These new types of homoclinic orbits were found with the homotopy technique of HomCont and then continued in the (ν_1, ν_2)-plane.

The curve h_1^a starts at the saddle-node bifurcation curve S_0 at a codimension-two non-central saddle-node homoclinic point to the left of SNH^-. Here, a *non-central homoclinic point* is a codimension-two bifurcation where the homoclinic orbit does not both depart from and return to one of the center manifolds of the saddle-node equilibrium it is connected to; see also [19]. It runs roughly parallel with h_0^a and also ends at the Hopf bifurcation curve H when the saddle focus a bifurcates. The curve h_1^b starts at a codimension-two non-central saddle-node homoclinic point to the right

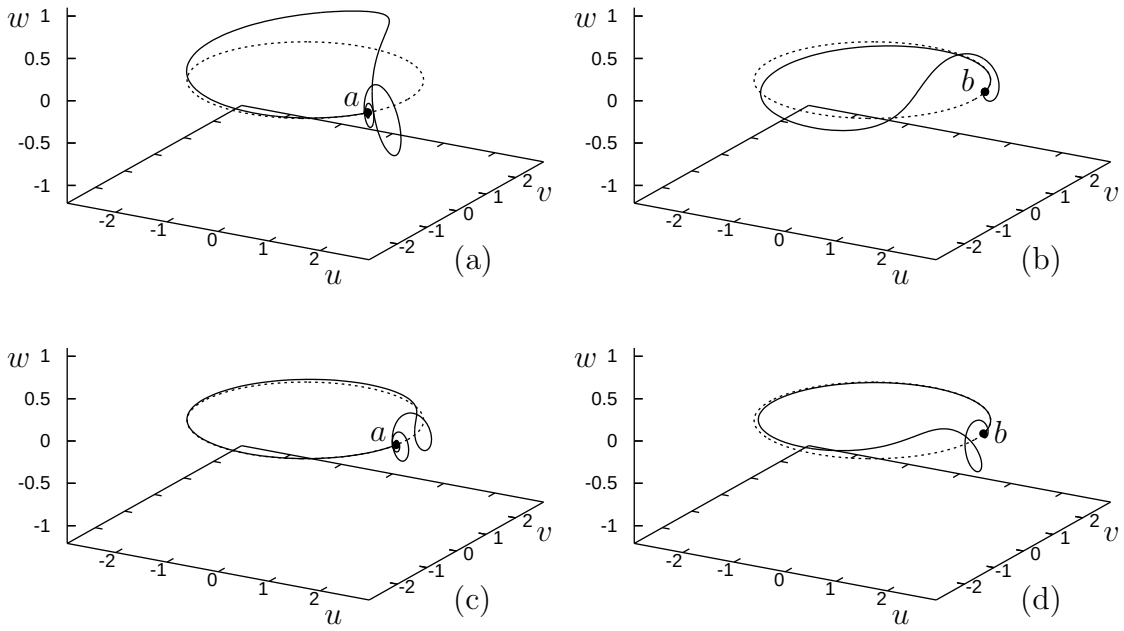

Figure 5. Homoclinic orbits of types h_1^a (a) and h_1^b (b) for $d = 0.01$, and h_1^a (c) and h_1^b (d) for $d = 0.001$ in (u, v, w)-space of (7); the dashed curve is the circle $\mathbb{S}^1 = \{z = 0\}$.

of SNH^-. It folds back and, close to the curve H, starts to oscillate and appears to accumulate on a line segment; see Figure 4(b). As was the case for h_0^b, the homoclinic orbit h_1^b accumulates on a saddle periodic orbit in the process; see section 5 for details of this phenomenon.

When one looks at figure 4 one notices that the curves h_1^a and h_1^b start and end quite 'far away' from the point SNH^-. The question arises whether h_1^a and h_1^b are an integral part of the unfolding of the SNH bifurcation with global reinjection. To show that this is indeed the case we consider what happens to the bifurcation diagram in the limit of invariant $\mathbb{S}^1$, that is, for $d \to 0$. Figure 6 gives an impression of the convergence process by showing the bifurcation diagram for the 10 times smaller value of $d = 0.001$.

By comparing figure 4(a) and figure 6(a) one notices the following. The local part of the bifurcation diagram, namely the curves S_0, H and S_l, remain unchanged; see Lemma 1. Furthermore, the curves h_0^a and h_0^b are much closer together; see figure 6(b). Indeed, it is known that for $d \to 0$ both h_0^a and h_0^b converge to a single curve C of a heteroclinic connection of the planar vector field model [6, 17].

Importantly, also the curves h_1^a and h_1^b move much closer to the 'central structure' of the bifurcation diagram. For example, unlike before, the curve h_1^b now intersects the curves h_0^a and h_0^b in several places; see figure 6(b). Furthermore, for decreasing d the global excursion of h_1^a and h_1^b follow the circle $\mathbb{S}^1$ more closely, as is clearly visible in figure 5(c) and (d), which depict these homoclinic orbits for $d = 0.001$. We remark that

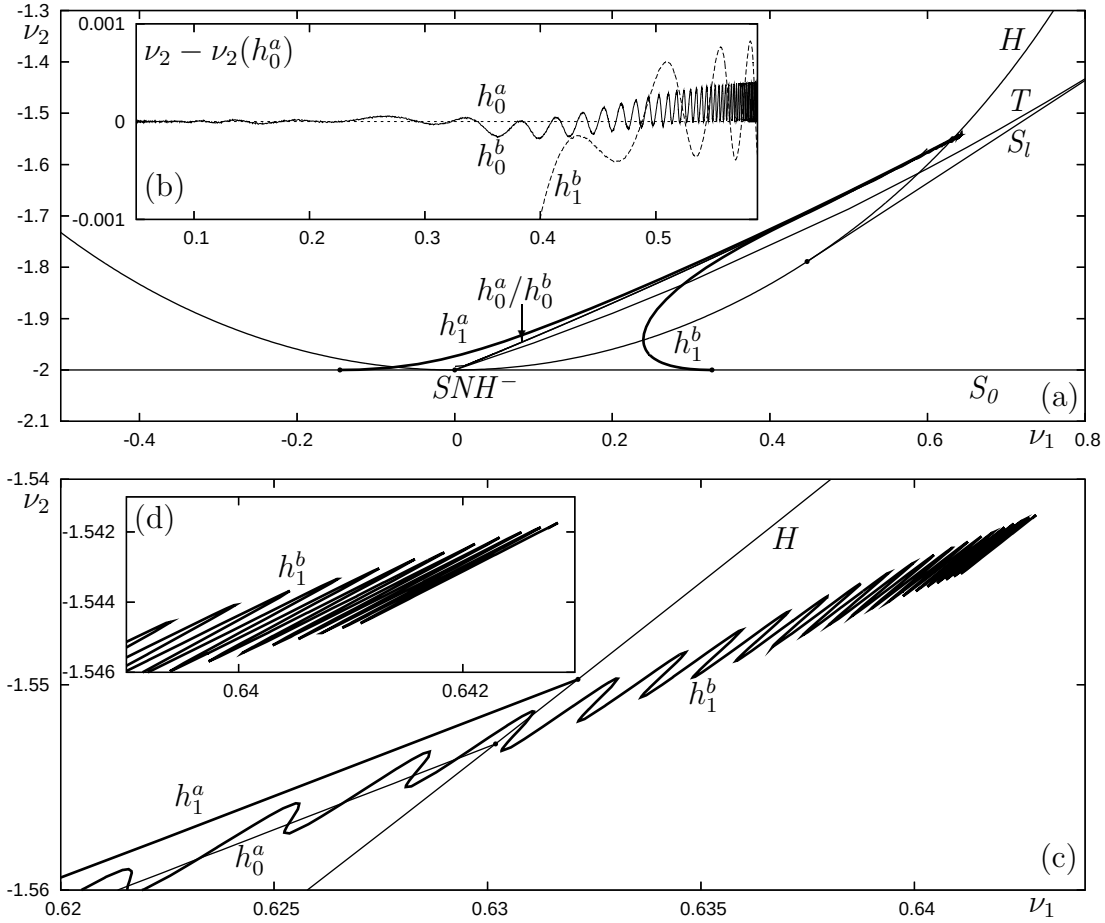

Figure 6. Bifurcation diagram in the (ν_1, ν_2)-plane near SNH^- for d=0.001; compare with figure 4. The insets (b) and (d) show details of how the curves h_0^b and h_1^b end. Since h_0^a and h_0^b are extremely close to each other, the curves in inset (b) are plotted relative to the curve h_0^a which, hence, appears as a straight line.

global reinjection homoclinic bifurcations appear to be very sensitive to breaking the invariance of $\mathbb{S}^1$. Therefore, we need to work with quite small values of d, which makes the numerical continuation of such homoclinic orbits quite challenging. Overall, figure 6 is numerical evidence that both h_1^a and h_1^b also approach the curve C of a heteroclinic connection of the planar vector field model (1).

4.3. Multiple-excursion homoclinic orbits

Homoclinic orbits may have not just one but multiple global excursions. To find and follow such orbits numerically we use the homoclinic branch switching technique described in [22], which is available with AUTO/HomCont [10]. We modified the branch switching algorithm so that it works in the covering space and recognizes the periodicity of the variable φ. To maintain accuracy, the more global excursions the orbit makes the more mesh points `NTST` we use in the AUTO computations.

Figure 7 shows the relevant part of the bifurcation diagram with homoclinic

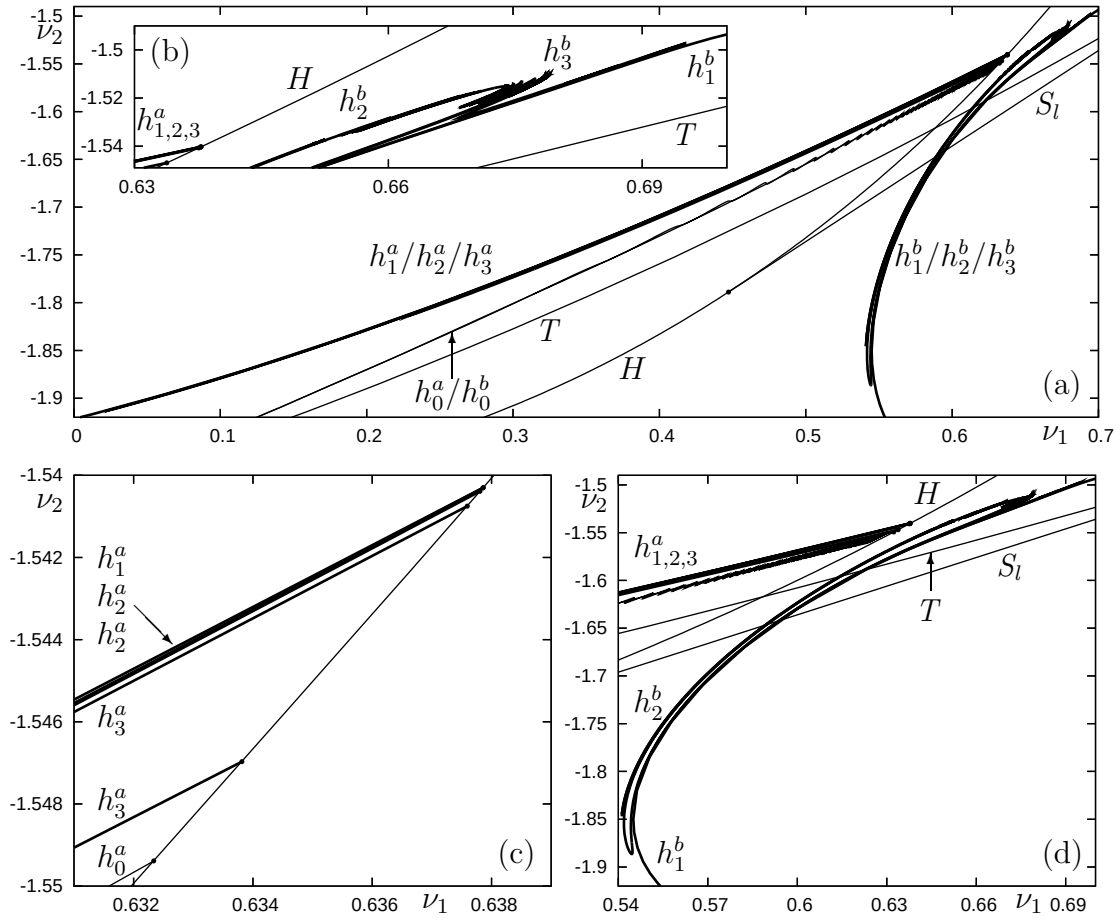

Figure 7. Bifurcation diagram in the (ν_1, ν_2)-plane near SNH^- for d=0.01 near the curves h^a_2, h^b_2, h^a_3 and h^b_3. Panel (b) is an enlargement near the end points of these curves, panel (c) shows how h^a_2 and h^a_3 end on H, and panel (d) shows h^b_2 and h^b_3 near h^b_1.

bifurcation curves h^a_2, h^b_2, h^a_3 and h^b_3 added; compare with figure 4. Phase portraits of the homoclinic orbits of types h^a_2, h^b_2, h^a_3 and h^b_3 are shown in figure 8(a)–(d), where one can clearly identify the different homoclinic orbits in terms of the number of global excursions along the (dashed) circle $\mathbb{S}^1$. The overview in figure 7(a) shows that the curves of homoclinic orbits of equilibrium a all lie very close to the curves h^a_1. The curves h^a_2 and h^a_3 start and end at homoclinic Hopf bifurcations on the curve H; see figure 7(c). They follow h^a_1 closely towards smaller values of ν_1 and then turn around back to H in a fold (with respect to ν_1). In other words, unlike the curve h^a_1, the curves h^a_2 and h^a_3 do not reach the saddle-node curve S_0. The curves h^b_2 and h^b_3 appear to start in some accumulation process near the Hopf curve H, follow h^b_1 towards lower values of ν_2 and then turn around in a fold (with respect to ν_2) back to the same region where they end in another accumulation process; see figure 7(b) Hence, they also do not reach the saddle-node curve S_0; see figure 7(d).

Since it is very difficult to determine the exact nature of h^b_2 and h^b_3 from the

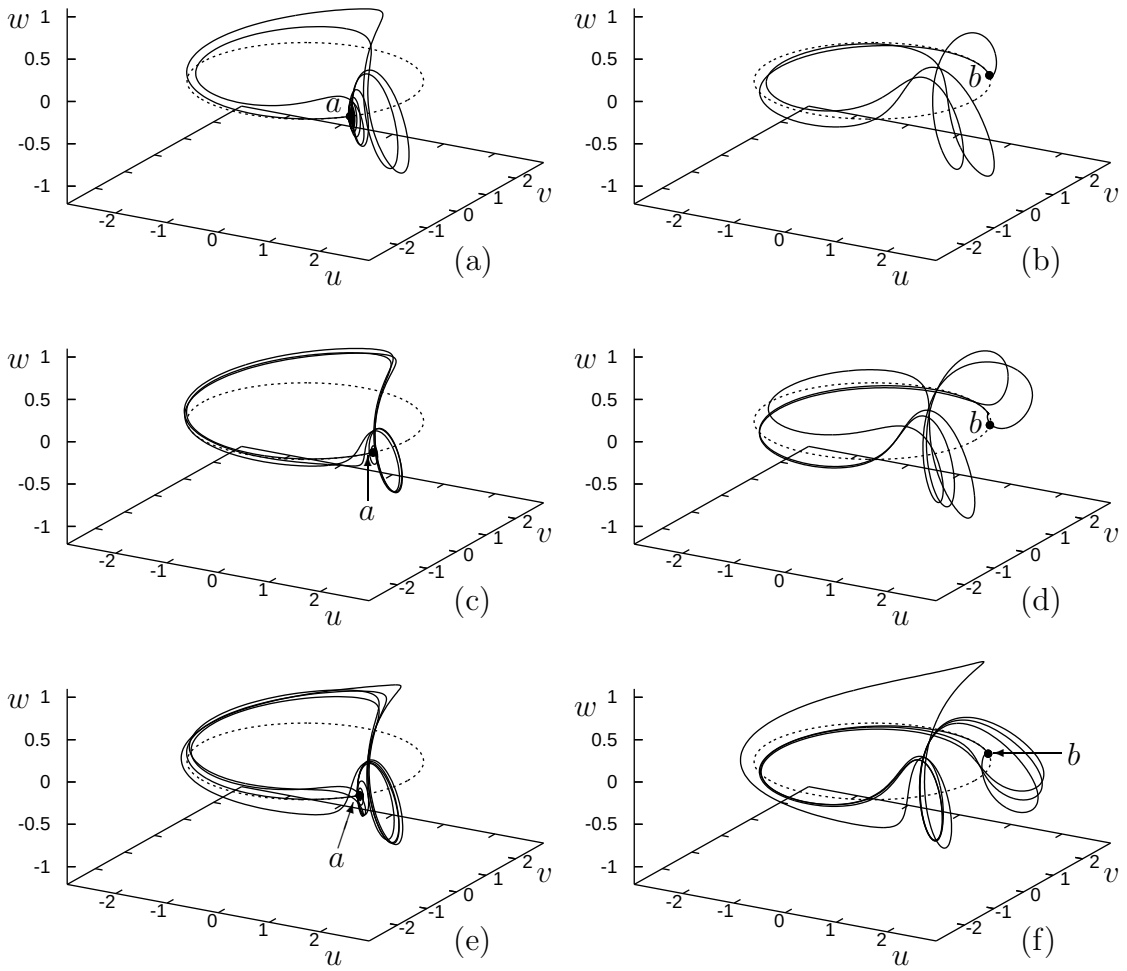

Figure 8. Homoclinic orbits of types h_2^a (a), h_2^b (b), h_3^a (c), h_3^b (d), h_4^a (e), and h_4^b (f) for $d = 0.01$ in (u, v, w)-space of (7); the dashed curve is the circle $\mathbb{S}^1 = \{z = 0\}$.

enlargements in figure 7, we show in figure 9 plots of the curves h_2^b and h_3^b relative to the curve h_1^b. This means that we plot the distance in ν_1 to the curve h_1^b, which appears as the (dotted) straight vertical line in figure 9(a). The curve h_2^b is the solid curve in figure 9. It seems to start and end in an accumulation process, but panels (a) and (b) of figure 9 together reveal that it is actually a single closed curve. The curve h_2^b starts to oscillate (both on the left and on the right) as part of an accumulation process as we have seen for the curve h_1^b in figure 4 and figure 6. However, the accumulation process is not complete and the two oscillations 'join up'. The phase portrait in Figure 9(c) of h_2^b at the marked 'connection point' shows that the homoclinic orbit makes a finite, maximal number of loops around a saddle periodic orbit.

Figure 9(a) shows that there are actually two (dashed) separate curves of homoclinic orbits of type h_3^b, both hugging the curve h_2^b. The lower left curve h_3^b is a simple,

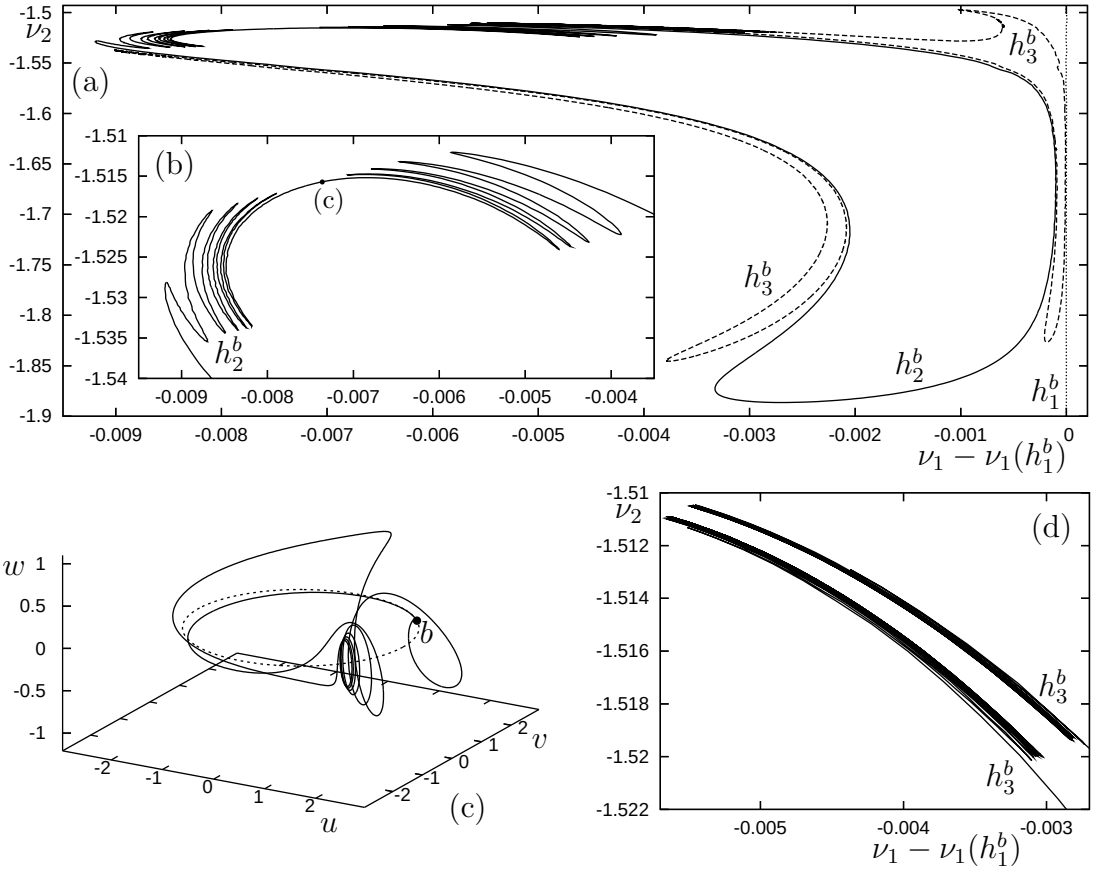

Figure 9. The curves h_2^b and h_3^b plotted relative to the curve h_1^b; compare with figure 7. Panels (b) is an enlargement of oscillations of the curve h_2^b, panel (c) shows the homoclinic orbit of type h_2^b in between these oscillations, and panel (d) is an enlargement of oscillations of the curve h_3^b.

banana-shaped curve — the respective homoclinic orbit does not interact with a saddle periodic orbit. However, the upper right curve appears to show an accumulation process. Figure 9(d) is a magnification in the relevant region of the (ν_1, ν_2)-plane. The situation looks somewhat similar to that in figure 9(b), but the two ends of the curve h^3 do not close up. Instead, they accumulate on two different segments. We stress that the numerical continuation was done very carefully to ensure that the difference between figure 9(b) and figure 9(d) is genuine.

It is possible with our branch switching method to find homoclinic orbits with even more global excursions. As an example, figure 8(e)–(f) shows homoclinic orbit of type h_4^a and h_4^b. The respective curves are not included in figure 7 because, as we have checked, the respective homoclinic bifurcation curves are even closer to the curves in figure 7 of homoclinic bifurcations with up to three global excursions. Furthermore, the continuation of homoclinic orbits with more than three global excursions becomes increasingly challenging. In fact, computing the curves h_0^a/h_0^b up to h_3^a/h_3^b reliably already required great numerical accuracy and a careful representation of the data.

5. Accumulation process of homoclinic bifurcation curves

In our investigation of the bifurcation diagram of (2) we have found that curves of homoclinic bifurcations of equilibrium b typically end by accumulating on a segment. At the same time, the homoclinic orbit itself approaches a saddle periodic orbit Γ. This codimension-one phenomenon, which we call a *codimension-one Equilibrium to a Periodic orbit (EtoP) heteroclinic cycle bifurcation*, has been studied theoretically in [23] from an abstract bifurcation theory point of view. The phenomenon is of codimension one because one of the connections of the EtoP cycle is of codimension zero (a generic intersection between the two-dimensional unstable manifold $W^u(b)$ of the equilibrium b and the two-dimensional stable manifold $W^s(\Gamma)$ of the periodic orbit Γ), while the other connection is of codimension one (the one-dimensional stable manifold $W^s(b)$ lies in the two-dimensional unstable manifold $W^u(\Gamma)$). Our investigation suggests, but this is not proved here or in [23], that this bifurcation occurs in two-dimensional parameter (ν_1, ν_2)-plane along a codimension-one curve segment, which starts and ends at points where an extra codimension-one bifurcation takes place. Namely, at the end points we expect a codimension-one heteroclinic tangency between $W^u(b)$ and $W^s(\Gamma)$, which bounds the region where the codimension-zero heteroclinic connection of the EtoP cycle from b to Γ exists. We remark that [23] is mainly concerned with the analysis of a more complicated codimension-two EtoP cycle bifurcation in a four-dimensional phase space.

The figures presented here are the first examples of what a codimension-one EtoP cycle bifurcation actually looks like in a concrete system. In this section we discuss in more detail the 'cleanest' example. Figure 10 shows the EtoP cycle bifurcation in which the curve h_1^b for $d = 0.01$ in figure 4 ends. A magnification near the accumulation process of h_1^b is shown figure 10(a). The maxima and the minima (with respect to ν_2) of h_1^b converge to separate points. Consequently, the ω-limit set of h_1^b is a curve segment that is bounded by the limits of the maxima and minima. In the accumulation process of the parameter curve h_1^b, the corresponding homoclinic orbit accumulates on a saddle periodic orbit (which bifurcates from the equilibrium a along the curve H). Two examples of such homoclinic orbits are shown in figure 10(c) and (d) in phase space and as time profiles. While it is difficult to see this in phase space, the time profile clearly shows that from maximum to maximum the orbit h_1^b surrounds the periodic orbit one more time before leaving its neighbourhood along its unstable manifold; note also the (exponential) decay of the maxima and minima of the time traces in figure 10(c2) and (d2).

The theory in [23] predicts that the accumulation process involves curves of saddle-node bifurcations of limit cycles, and we indeed found many of them by following periodic orbits that bifurcate from h_1^b. Figure 10(b) shows an example of such a curve, labelled S_l. The curve S_l has several cusp bifurcation points, so that it 'surrounds' the region where the accumulation of h_1^b occurs. We found that this is the typical structure of saddle-node bifurcation of limit cycles curves that are associated with the accumulation process. Figure 10(e) shows the saddle-node periodic orbit in phase space and as a time

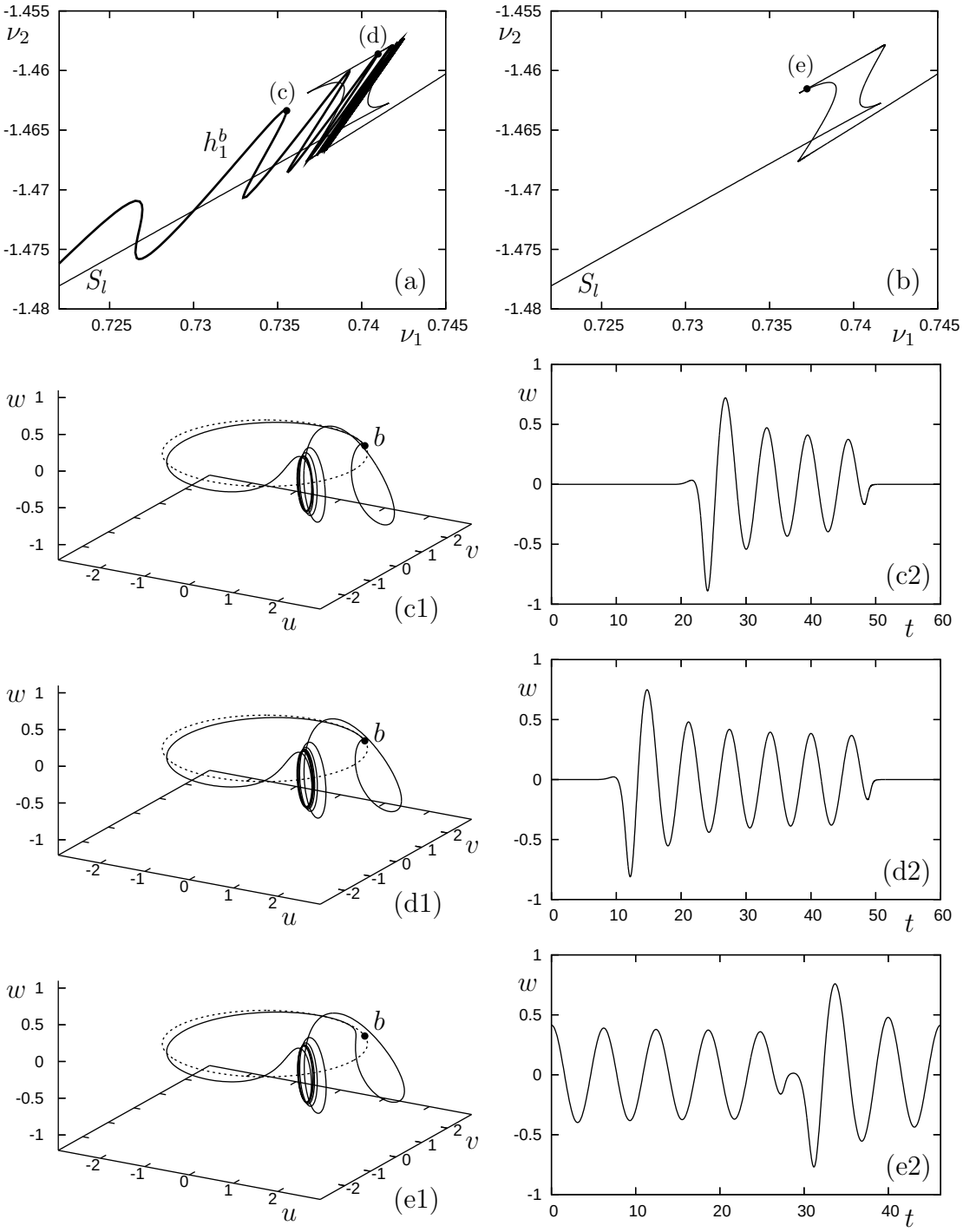

Figure 10. The curve h_1^b accumulates on a line segment (a) while the homoclinic orbit itself accumulates on a saddle-periodic orbit; panels (c) and (d) show homoclinic orbits of type h_1^b in (u, v, w)-space (left) and time profile (right) as computed with AUTO/HomCont. Panel (b) shows a nearby saddle-node bifurcation curve of limit cycles S_l, and panel (e) is an example of a saddle-node periodic orbit.

i	dist(i)	dist(i)/dist($i-1$)
1	0.0119280257	
2	0.0049877450	0.418153
3	0.0022378597	0.448671
4	0.0010476684	0.468156
5	0.0005055581	0.48255
6	0.0002461077	0.48680
7	0.0001219180	0.49538

Table 1. Distances dist(i) between the ith and the $(i-1)$st maximum of the curve h_1^b for $d = 0.01$ and their ratios; the point marked (c) in figure 10(a) is the first maximum. As predicted by theory [23], the ratio approaches the stable Floquet multiplier 0.498061 of the saddle periodic orbit on which the homoclinic orbit accumulates.

profile. Note that the one larger maximum corresponds to the global excursion around the (dashed) circle $\mathbb{S}^1$.

We end this section by considering the scaling of the accumulation process of the curve h_1^b onto its ω-limit set. According to [23], in the codimension-two case consecutive maxima (or minima) converge to their limit with a rate given by the stable eigenvalue of the saddle periodic orbit Γ of the EtoP cycle. Preliminary theoretical investigations‡ suggest that the same is true for the codimension-one case. The Floquet multipliers of Γ, as determined with AUTO, are 0.4980612, 1 and 636.037. Table 1 contains data of the distances dist(i) between the ith and the $(i-1)$st maximum of the curve h_1^b in figure 10(a), where maximum (c) is that for $i = 1$. The numbers dist(i) were determined as the Euclidean distances between fold points (`LP`) detected by AUTO/HomCont during continuation of the curve h_1^b. To resolve this curve we used the fairly high value of `NTST`= 400 mesh points to account for the complexity of the homoclinic orbit as it approaches the saddle periodic orbit Γ. In this way, we were able to determine the first six ratios dist(i)/dist($i-1$) in the last column of table 1. The ratios indeed converge within numerical accuracy to the stable Floquet multiplier 0.498061.

6. Discussion and conclusions

We constructed a three-dimensional model vector field of a saddle-node Hopf bifurcation with global reinjection. Starting from what is known about a planar vector field approximation, we considered the two-parameter bifurcation diagram for the well-known case of a SNH point of type III. Of special interest are bifurcations of periodic and homoclinic orbits orbits that make one or more global excursions out of and back into a neighbourhood of the SNH point. We used AUTO/HomCont and a specialized homoclinic branch switching method to actually find and follow such multi-excursion homoclinic orbits. This revealed an intricate bifurcation structure that must be expected

‡ by A.R. Champneys, V. Kirk, E. Knobloch, B.E. Oldeman; and J.D.M. Rademacher; to be published.

near SNH point (of type III) with global reinjection. Due to the global nature of the problem, the model vector field cannot be expected to yield a generic unfolding. However, similar to the results in [15], small parameter changes will only affect global bifurcations outside a neighbourhood of the type III SNH point. For example, the curve h_0^a may terminate using a different global mechanism than a homoclinic Hopf bifurcation. In other words, we expect the global reinjection homoclinic orbits to be rather robust.

From an abstract point of view one would expect to find even more types of global reinjection orbits when the invariant sphere, the (local) connection inside the sphere, and the global connection (excursion) along $\mathbb{S}^1$ outside the sphere are broken. An open problem is the construction of homoclinic orbits that combine global excursions with 'local excursions'. Starting points for constructing numerical starting data for such orbits may be crossing points of the curves h_0^a and h_1^b (as found in figure 4), where the system has both types of homoclinic orbits. However, this is numerically a very difficult problem since we found these crossing points only very close to the limit when the circle $\mathbb{S}^1$ is invariant.

As a particular feature of the bifurcation diagram we found a codimension-one EtoP cycle bifurcation — an accumulation phenomenon where a homoclinic orbit accumulates on a saddle periodic orbit. Our results show that this bifurcation, which was studied theoretically in [23], occurs naturally in the unfolding of a SNH point (of type III) with global reinjection. In our model vector field we found good agreement with the theory, including the scaling of the accumulation process. We remark that accumulating homoclinic orbits have also been found in slow-fast vector field models from cell dynamics; see for instance [25]. However, due to the slow-fast nature, the analysis and even the computation of homoclinic orbits, let alone scaling laws, is much more difficult in the slow-fast context. The vector field model presented here does not suffer from these difficulties.

An interesting question for further research is how two separate EtoP cycle bifurcations may start to interact. This question is motivated by two examples that we found — one where two such bifurcations are very close together, and one where the accumulation of the global homoclinic orbit on a saddle periodic orbit appears to be 'incomplete'. It seems that, upon the variation of an additional parameter, these two cases can be transformed into each other by (an infinite number of) transitions through saddle singularities in the surface of homoclinic orbits. This conjecture is inspired by similar bifurcation scenarios that were recently found near extrema of curves of T-point and double-homoclinic bifurcations [1, 29].

While the model vector field is not (and cannot be) an unfolding of this global bifurcation, multi-excursion orbits must be expected in applications that feature SNH points with global reinjection. For example, in a semiconductor laser with optical injection a global excursion corresponds to a phase slip between the laser and the injected optical field. It is an interesting topic for future research to identify multi-excursion (or multi-phase slip) periodic and homoclinic orbits is this laser system. Of special interest will be the relationship of multi-excursion homoclinic orbits with a complex bifurcation

structure that gives rise to multi-pulse excitability [29, 31].

Acknowledgements

The authors thank Vivien Kirk and Jens Rademacher for stimulating discussions. The research of B.K. was supported by an EPSRC Advanced Research Fellowship grant and that of B.E.O. by a postdoctoral fellowship from the New Zealand Institute of Mathematics and its Applications (NZIMA).

References

[1] Algaba A, Merino M, Fernández-Sánchez F and Rodriguez-Luis A 2002 Closed curves of global bifurcations in Chua's equation: a mechanism for their formation *Int. J. Bifurcation and Chaos* **13**, 609–616.

[2] Algaba A, Merino M, and Rodriguez-Luis A 2001 Takens Bogdanov bifurcations of periodic orbits and Arnold's tongues in a three-dimensional electronic model *Int. J. Bifurcation and Chaos* **11**, 513–531.

[3] Ashwin P, Rucklidge A M and Sturman R 2004 Two-state intermittency near a symmetric interaction of saddle-node and Hopf bifurcations: a case study from dynamo theory *Physica D* **194**, 30–48.

[4] Broer H W and Vegter G 1992 Bifurcational aspects of parametric resonance *in* Dynamics Reported, New Series Vol. 1 Springer-Verlag pp. 1–51.

[5] Broer H, Roussarie R and Simo C 1993 On the Bogdanov-Takens bifurcation for planar diffeomorphisms *in* Perello C et al, eds. *Proc Equadiff '91* World Scientific, Singapore, 81–92

[6] Champneys A R and Kirk V 2004 The entwined wiggling of homoclinic curves emerging from saddle-node/Hopf instabilities *Physica D* **195**, 77–105.

[7] Champneys A R and Kuznetsov Yu A 1994 Numerical detection and continuation of codimension-two homoclinic bifurcations *Int. J. Bifurcation and Chaos* **4**(4), 785–822.

[8] Champneys A R, Kuznetsov Yu A and Sandstede B 1996 A numerical toolbox for homoclinic bifurcation analysis *Int. J. Bifurcation and Chaos* **6**(5), 867–887.

[9] Chow S N, Li C and Wang D 1994 *Normal Forms and Bifurcation of Planar Vector Fields* Cambridge University Press.

[10] Doedel E J, Paffenroth R C, Champneys A R, Fairgrieve T F, Kuznetsov Yu A, Oldeman B E, Sandstede B and Wang X 2001 *AUTO 2000: Continuation and Bifurcation Software for Ordinary Differential Equations (with HomCont).* `http://sourceforge.net/projects/auto2000/`.

[11] Gaspard, P 1993 Local birth of homoclinic chaos *Physica D* **62**(1-4), 94–122.

[12] Guckenheimer J and Holmes P 1983 *Nonlinear Oscillations, Dynamical Systems and Bifurcations of Vector Fields* Springer-Verlag.

[13] Kirk V 1991 Breaking of symmetry in the saddle-node Hopf bifurcation *Phys. Lett. A* **154**, 243–248.

[14] Knobloch E and Moore D 1990 Minimal model of binary fluid convection *Physical Review A* **42**(8), 4693–4709.

[15] Krauskopf B and Oldeman B E 2004 A planar model system for a saddle-node Hopf bifurcation with global reinjection *Nonlinearity* **17**, 1119-1151.

[16] Krauskopf B, Tollenaar N and Lenstra D 1998 Tori and their bifurcations in an optically injected semiconductor laser *Optics Communications* **156**(1–3), 158–169.

[17] Krauskopf B and Rousseau C 1997 Codimension-three unfoldings of reflectionally symmetric planar vector fields *Nonlinearity* **10**, 1115–1150.

[18] Krauskopf B and Wieczorek S M 2002 Accumulating regions of winding periodic orbits in optically driven lasers *Physica D* **173**, 97–113.
[19] Kuznetsov Yu A **2004** *Elements of Applied Bifurcation Theory* 3rd edn (New York: Spinger).
[20] Moroz I 1990 Multiple instabilities in rotating convection *Geophys. Astrophys. Fluid Dynamics* **53**, 183–204.
[21] Mullin T, Tavener S J and Cliffe K A 1989 An experimental and numerical study of a codimension-2 bifurcation in a rotating annulus *Europhysics Letters* **8**(3), 251–256.
[22] Oldeman B E, Champneys A R and Krauskopf B 2003 Homoclinic Branch Switching: A numerical implementation of Lin's method *Int. J. of Bifurcation and Chaos* **10**, 2977–2999.
[23] Rademacher J D M 2005 Homoclinic orbits near heteroclinic cycles with periodic orbits *Journal of Differential Equations*, in press.
[24] Shil'nikov A, Nicolis G and Nicolis C 1995 Bifurcation and predictability analysis of a low-order atmospheric circulation mode *Int. Journal of Bifurcation and Chaos* **5**, 1701–1711.
[25] Simpson D, Kirk V and Sneyd J 2005 Complex oscillations and waves of calcium in pancreatic acinar cells. *Physica D* **200**, 303–324.
[26] Solari H G and Oppo G L 1994 Laser with injected signal: Perturbation of an invariant circle *Optical Communications* **111**, 173–190.
[27] Sneyd J, LeBeau A and Yule D 2000 Travelling waves of calcium in pancreatic acinar cells: model construction and bifurcation analysis *Physica D* **145**, 158–179.
[28] Vitolo R 2003 Bifurcations of attractors in 3D diffeomorphisms: a study in experimental mathematics *PhD Thesis* University of Groningen.
[29] Wieczorek S M and Krauskopf B 2005 Bifurcations of n-homoclinic orbits in optically injected lasers *Nonlinearity* **18**(3), 1095–1120.
[30] Wieczorek S M, Krauskopf B, Simpson T B and Lenstra D 2005 The dynamical complexity of optically injected semiconductor lasers *Physics Reports* **416**(1–2), 1–128.
[31] Wieczorek S M, Krauskopf B and Lenstra D 2002 Multipulse excitability in a semiconductor laser with optical injection *Phys. Rev. Lett.* **88**(6), 063901.
[32] Zimmermann M, Natiello M and Solari H 1997 Shil'nikov-saddle-node interaction near a codimension 2 bifurcation: laser with injected signal *Physica D* **109**, 293–314.